Regulation of cerebrospinal fluid and brain tissue sodium levels by choroid plexus and brain capillary endothelial cell Na^+, K^+-ATPases during migraine

Hamed Ghaffari[1,a], Samuel C. Grant[2], Linda R. Petzold[1], Michael G. Harrington[3]

[1)] Department of Mechanical Engineering, University of California Santa Barbara, Santa Barbara, CA, USA.
[2)] Department of Chemical and Biomedical Engineering, FAMU-FSU College of Engineering, Tallahassee, FL, USA
[3)] Molecular Neurology Program, Huntington Medical Research Institutes, Pasadena, CA, USA.

[a)] To whom correspondence should be addressed. Email: hamed_ghaffari@ucsb.edu

Abstract

Background

It is known that sodium concentration in both cerebrospinal fluid (CSF) and brain interstitial fluid (ISF) increases during migraine. However, little is known regarding the underlying mechanisms of sodium homeostasis disturbance in the brain during the onset and propagation of migraine. Exploring the cause of sodium dysregulation in the brain is important, since correction of the altered sodium homeostasis could potentially treat migraine.

Methods

Under the hypothesis that disturbed homeostasis of brain capillary endothelial cells (CEC) and choroid plexus (CP) Na^+, K^+-ATPase (NKAT) is the underlying cause of the elevated CSF and ISF sodium levels in migraine sufferers, we developed a mechanistic, differential equation model of a rat's brain to compare the significance of CP and CEC NKATs in controlling CSF and ISF sodium levels. The model includes the ventricular system, subarachnoid space, brain tissue, plasma and CP. The activity levels of CP and CEC NKATs are modeled by permeability coefficients of CP and CEC to sodium, respectively. We then performed a global sensitivity analysis to investigate the significance of CEC and CP permeabilities to sodium in controlling CSF and ISF sodium concentrations.

Results

We show that the variation of permeability of CP to sodium is much more important than the alteration of CEC permeability to sodium in controlling CSF and ISF sodium levels. Our

simulations indicate that the sodium flux at the interface of the ventricular system and brain tissue is greater than the sodium flux at the contact surface of the brain tissue and subarachnoid space during an episode of migraine.

Conclusions

Using mathematical modeling, we demonstrate that overactivity of CP NKATs has a more significant effect than overactivity of CEC NKATs on ISF and CSF sodium concentrations. Our results suggest that altered homeostasis of CP NKATs is a potential cause of migraines in the rats. Further studies on CP NKAT activity levels during migraine episodes with different triggers can help better understand migraine pathophysiology.

Keywords

Migraine, Sodium, Na^+, K^+-ATPase, Cerebrospinal fluid, Choroid plexus, Brain capillary endothelial cell, Computational model, Global sensitivity analysis, Sobol's method

1. Introduction

Migraine is ranked among the top five causes of disability in the world [1]. Although the exact underlying causes of migraine are not known, common triggers of migraine include dehydration, stress, sleep disorders, hunger, etc. Understanding the pathophysiology of migraine is challenging because migraine triggering is different for everyone. Many of the triggers of migraine change the sodium balance in the brain. Previous animal and human studies [2-4] have revealed that migraine sufferers have higher levels of cerebrospinal fluid (CSF) and brain interstitial fluid (ISF) sodium than control groups, while there is no significant difference between plasma concentration of sodium in migraineurs and healthy controls. Previous studies have indicated that elevated levels of ISF sodium increase neuronal excitability [5], which subsequently results in migraine [6]. It has been suggested that the high levels of CSF and ISF sodium concentrations in migraineurs are due to a disturbance in the homeostasis of NKATs on the choroid plexus (CP) and brain capillary endothelial cells (CEC) [7]. NKATs are highly-conserved membrane proteins which are expressed in all cells. NKATs, which consume approximately 50% of the energy in the brain, maintain the physiological sodium and potassium electrochemical gradients across the cell membrane. An NKAT pumps 3 sodium ions out of the cell for every 2 potassium ions entering the cell. Overactivity of CEC and CP NKATs can increase the rate of sodium transport from plasma to the CSF and ISF. However, the extent of contribution of CEC and CP NKATs to the elevated CSF and ISF sodium concentrations has yet to be determined. Experimental study of the roles and significance of various NKATs in regulating ISF and CSF sodium levels is challenging because NKAT activity levels can be affected differently in response to various migraine triggers, as well as in response to the same migraine trigger from rat to rat. In this work, we use mechanistic modeling together with global sensitivity analysis (GSA) to deal with this uncertainty and lack of information. We develop a mathematical model to study the dynamics of sodium distribution in the brain following a perturbation in the activity levels of CEC and CP NKATs. Our model consists of four compartments: the ventricular system, subarachnoid space, brain tissue and plasma. We perform a GSA to assess the significance of CP and CEC NKATs in controlling sodium concentrations in the ISF and ventricular CSF. Our results reveal that the permeability coefficient of the CP to sodium is a more sensitive model parameter than the permeability coefficient of CEC to sodium.

The computational model presented in this study can not only shed light on the dynamics of sodium exchange between CSF, ISF and plasma, but also can be used to simulate the effects of different migraine triggers on NKATs and subsequently on sodium distribution in the brain. To accomplish such a task, further biological information regarding the variations in the functions of NKATs during an episode of migraine is needed.

2. Methods

2.1. Model Development

We modeled a rat's brain by three concentric spheres representing the ventricular system, brain tissue and subarachnoid space (Fig. 1). Brain tissue was modeled as a single compartment. We assumed that blood vessels are distributed randomly, following a uniform distribution, throughout the brain tissue [8-11].

Figure 1.

The inner sphere, which represents the ventricular system, includes the CP. CSF is secreted by the CP, flows into the ventricular system, and then passes through small openings (foramina) into the subarachnoid space where it is absorbed through blood vessels into the bloodstream. For simplicity, in our model we have assumed that the CSF secretion rate is equal to the CSF absorption rate from the subarachnoid space to the plasma. We have also assumed that sodium can be freely exchanged between the ISF and the CSF at the interface of brain tissue and the ventricular system, and at the contact surface of the subarachnoid space and brain tissue (dashed circles in Fig. 1b). This is due to the negligible permeability barrier of the contact surfaces. Sodium is also exchanged between plasma and the ISF through CEC, and can also diffuse in the brain ISF down its concentration gradient.

2.2. Formulation of the model

Ventricular and extracerebral sodium concentrations were modeled by ordinary differential equations (ODEs) represented by Eqs. 1-2, while the variation of sodium concentration across brain tissue was modeled by a partial differential equation (PDE), represented by Eq. 3.

$$\frac{\partial C_v(t)}{\partial t} = \frac{P_{cp}A_{cp}}{V_v}C_{pl} - \frac{P'_{cp}A_{cp}}{V_v}C_v + \frac{P_{vb}A_v\lambda}{V_v}\left(\frac{C_{br}(t,r_i)}{V_{br}} - C_V\right) - \frac{Q_{csf}}{V_v}C_v \qquad 0 \le t \le 2 \qquad (1)$$

$$\frac{\partial C_s(t)}{\partial t} = \frac{P_{sb}A_s\lambda}{V_s}\left(\frac{C_{br}(t,r_o)}{V_{br}} - C_s\right) + \frac{Q_{csf}}{V_s}C_v - \frac{Q_{csf}}{V_s}C_s \qquad 0 \le t \le 2 \qquad (2)$$

$$\frac{\partial C_{br}(t,r)}{\partial t} = P_{bc}A_{bc}C_{pl} - \frac{P'_{bc}A_{bc}}{V_{br}}C_{br} + \frac{\lambda}{\rho V_{br}r^2}\frac{\partial}{\partial r}\left(Dr^2\frac{\partial C_{br}}{\partial r}\right), \qquad r_i < r < r_o \qquad (3)$$

where C_v, C_s, C_{pl} and C_{br} represent ventricular sodium concentration, extracerebral sodium concentration, plasma sodium concentration and sodium level in brain tissue, respectively. C_v, C_s and C_{pl} are expressed in mole ml^{-1}, while C_{br} is defined as moles of sodium per gram of brain (mole g^{-1}). The ISF sodium concentration (mole ml^{-1}) was estimated by $\frac{C_{br}}{V_{br}}$ [8]. The model's parameters are defined in Table 1. The parameters r_i and r_o, which specify the boundaries of brain tissue (Fig. 1b), were obtained via the relationships

$$V_v = \frac{4}{3}\pi {r_i}^3 \qquad (4)$$

and

$$V_v + V_b = \frac{4}{3}\pi {r_o}^3, \qquad (5)$$

where V_v and V_b represent the ventricular system volume and brain tissue volume, respectively.

The terms on the left-hand side of Eqs. 1 and 2 represent the rate of change of sodium concentration (mole ml^{-1}) in the ventricular and extracerebral CSF, respectively, while the term on the left-hand side of Eq. 3 represents the rate of change of sodium level (mole g^{-1}) in the brain tissue. The four terms on the right-hand side of Eq. 1 represent sodium transport from the plasma to the ventricular CSF, sodium transport from the ventricular CSF to the plasma, sodium exchange between the ventricular CSF and the brain tissue, and sodium loss from the ventricular system due to bulk flow of CSF from the ventricular system to the subarachnoid space, from left to right, respectively. The

three terms on the right-hand side of Eq. 2 denote sodium exchange between the extracerebral CSF and the brain tissue, sodium input to the extracerebral CSF due to the bulk flow of CSF, and sodium loss from the subarachnoid space due to CSF absorption into the plasma, from left to right, respectively. The three terms on the right-hand side of Eq. 3 represent sodium transport from the plasma to the brain ISF, sodium transport from the brain ISF to the plasma, and diffusive transport of sodium across the brain tissue, from left to right, respectively.

The initial conditions for the ODEs (Eqs. 1-2) are given by

$$C_v = C_s = 145 \text{ mM}. \tag{6}$$

We have also assumed that C_{pl} is 140 mM at steady state.

Rates of exchange of sodium at the boundaries of Eq. 3 are defined by

$$Q_v = P_{vb} A_v \lambda \left(C_v - \frac{C_{br}(t,r)}{V_{br}} \right) \qquad r = r_i \tag{7}$$

$$Q_s = P_{sb} A_s \lambda \left(C_s - \frac{C_{br}(t,r)}{V_{br}} \right). \qquad r = r_o \tag{8}$$

We used large values for P_{sb} and P_{vb} due to the negligible permeability barrier of the contact surfaces to sodium. Thus, the ISF sodium concentration is approximately in equilibrium with ventricular and extracerebral sodium concentrations at the interface of brain tissue and CSF. A_v and A_s represent the contact surface area of the brain tissue and the ventricular system, and the contact surface area of the brain tissue and the subarachnoid space, respectively. The contact surfaces were modeled as concentric spheres with the radiuses of r_i and r_o (Fig. 1).

Equation 3 was coupled with Eq. 1 and Eq. 2 at the boundaries of brain tissue ($r = r_i$ and $r = r_o$), using Eq. 7 and Eq. 8, respectively.

Table 1. List of the model's parameters

Parameters	Description	Value	Reference
P_{cp}	CP permeability to sodium (from blood to CSF)	3.8×10^{-5} (cm s^{-1})	[8]
A_{cp}	Surface area of CP	1 (cm^2)	[8]
P'_{cp}	CP permeability to sodium (from CSF to blood)	Unknown	
V_s	Subarachnoid space volume	0.2 (ml)	[8, 12]
V_v	Ventricular system volume	0.1 (ml)	[8, 12]
V_b	Brain tissue volume	1.1 (ml)	[13]
P_{bc}	CEC permeability to sodium (from blood to ISF)	1.4×10^{-7} (cm s^{-1})	[8]
A_{bc}	Surface area of CEC	140 (cm^2 g^{-1})	[8]
P'_{bc}	CEC permeability to sodium (from ISF to blood)	Unknown	
V_{br}	Cerebral distribution volume of sodium	0.34 (ml g^{-1})	[8]
D	Diffusion coefficient of sodium in the ISF	1.15×10^{-5} (cm^2 s^{-1})	[14]
Q_{csf}	CSF flow rate	3.6×10^{-5} (ml s^{-1})	[8]
P_{vb}	Permeability coefficient of the contact surface of brain tissue and ventricular system to sodium	10^6 (cm s^{-1})	A large value was used
P_{sb}	Permeability coefficient of the contact surface of brain tissue and subarachnoid space to sodium	10^6 (cm s^{-1})	A large value was used
λ	ISF/brain volume fraction	0.2 (dimensionless)	[8, 15]
ρ	Rat brain density	1 (g ml^{-1})	[8]

P'_{cp} and P'_{bc} were calculated assuming that the CSF sodium level is in equilibrium with the ISF sodium concentration at t=0 (steady state):

$$C_{br}(t,r) = C_v \times V_{br} = C_s \times V_{br}. \qquad \text{for} \qquad r_i \le r \le r_o \qquad (9)$$

This assumption implies that there is no sodium exchange between the CSF and the brain tissue at the two contact surfaces of brain tissue and CSF at t=0 [16, 17].

To solve the system of differential equations described by Eqs 1-3, we discretized Eq. 3 with respect to the variable r using the central difference approximation, and we approximated the time derivatives via backward differences. The main advantage of this fully implicit scheme, a.k.a. backward time central space (BTCS), is that it is unconditionally stable.

In the next section, we perform a local sensitivity analysis to investigate how an increase in P_{cp} and P_{bc} affects brain and CSF sodium concentrations. We also perform a global sensitivity analysis (GSA) to further analyze the significance of P_{cp} and P_{bc} variations in controlling the levels of sodium in the CSF and brain tissue. Compared with local sensitivity analysis, which assesses the local impacts of variations of the model's parameters on the model's output, GSA assesses how the uncertainty of the model's output is apportioned to variations in multiple model inputs. Using GSA, we compare the importance of P_{cp} and P_{bc} in controlling brain tissue and CSF sodium concentrations, while we take into account the inter-subject variability in all of the model's parameters. We use a MATLAB toolbox for GSA, called SAFE [18]. We perform Sobol's sensitivity analysis, which quantitively ranks the relative importance of the parameters by decomposing the model's output variance into the contributions associated with each model's input. Sobol's method which has been widely applied to complex systems biology and pharmacology models [19-24], calculates the first-order and total-effect sensitivity indices for each model parameter. The first-order indices (S_i) measure the individual contributions of each input to the variance of the model output, while the total-effect indices (S_{Ti}) represent the total contribution of the input, including its first-order effect and all higher-order interactions (see Supplementary Information for details).

3. Results

It is believed that disturbed homeostasis in CEC and CP NKATs plays an important role in the initiation of migraine [7]. Increased activity of CP and CEC NKATs enhances sodium transport from blood to CSF and ISF. Overactive NKATs were modeled by elevated P_{cp} and P_{bc} in our

model. Figure 2 shows the variations in ISF, ventricular and extracerebral CSF sodium concentrations after a 20% increase in P_{cp}.

Figure 2.

Sodium starts to diffuse from blood to ventricular CSF after increasing the permeability of CP to sodium (Fig. 2a). We assumed that sodium exchange between plasma and CSF does not change plasma concentration of sodium significantly due to the large volume of plasma compared to CSF. Thus, C_{pl} remains unchanged after changing the permeability coefficient of CP to sodium. Elevated levels of sodium in the ventricular CSF lead to diffusion of sodium from CSF to ISF and distribution of sodium into the brain tissue over time (Fig. 2c). Sodium moves by bulk flow of CSF from the ventricular system to subarachnoid space where it can be exchanged between CSF and ISF. Extracerebral sodium concentration increases after increasing the permeability coefficient of CP to sodium, while this increase is less than the observed rise in ventricular sodium level (Fig. 2b). Figure 2 demonstrates that the ISF sodium concentrations at the contact surface of brain tissue and the ventricular system, and the contact surface of brain tissue and the subarachnoid space, are almost in equilibrium with the ventricular and extracerebral sodium concentrations, respectively. This is due to the negligible permeability barrier of the contact surfaces to sodium. However, sodium distribution across the brain tissue varies over time and space (Fig. 2c). Supplementary animation 1 shows the variations of ISF, ventricular and extracerebral sodium concentrations within 2 hours after perturbation of P_{cp}.

A 20% increase in CEC permeability to sodium enhances sodium transport from plasma to the ISF (Fig. 3c). The elevated levels of sodium in the ISF increases sodium transport from the ISF to the ventricular system and subarachnoid space (Fig. 3a-b). Supplementary animation 2 shows time-dependent changes in the ISF, ventricular and extracerebral sodium concentrations within 2 hours after increasing P_{bc} by 20%.

Figure 3.

Figure 4 shows sodium flux between the ISF and CSF at the interface of the brain tissue and the ventricular system and at the contact surface of the brain tissue and the subarachnoid space, after increasing P_{cp} or P_{bc} by 20%. Our results indicate that sodium flux from the ventricular system to the brain tissue is higher than sodium flux from the subarachnoid space to the brain tissue.

Figure 4.

Figure 2 and Figure 3 compare the variations of C_v, C_s, and C_{br} when a single parameter, i.e. P_{cp} or P_{bc}, is perturbed and the rest of the parameters remain unchanged. However, in the case of migraine, both the CP and CEC permeabilities, i.e. P_{cp} and P_{bc}, would most likely vary. Additionally, the model's parameters such as A_{cp}, V_s, V_v, V_b, etc can change across a population of rats of the same type. Thus, we used GSA [18] to consider the effects of variations in all model parameters. In this regard, we assumed that physiological concentration of sodium in CSF and plasma can vary within 5% of the *in vitro* values (i.e. $C_v = C_s = 145$ mM, $C_{pl} = 140$ mM), while the remaining independent model parameters can vary within 25% of the *in vitro* values (Table 1). Following a uniform distribution, we sampled 10^5 sets of parameters within their ranges of variability, which characterized different rats of the same type. We then calculated the dependent parameters, i.e. P'_{cp} and P'_{bc} for each set of parameters, assuming that the model is at steady state at t=0. We then assumed that P_{cp} and P_{bc} can change within 50% of the physiological values due to migraine triggers. We performed a GSA to investigate the significance of variations of P_{cp} and P_{bc} in controlling ventricular sodium concentration during episodic migraines. The model output was defined as the percent change of total ventricular sodium concentration within 2 hours after perturbations of P_{cp} and P_{bc}:

$$\text{Model Output}=\frac{\left(\frac{\int_0^{t_{max}} C_v\,dt}{t_{max}}\right)-C_v(t=0)}{C_v(t=0)}$$

Our results indicate that the variation of P_{cp} is much more important than that of P_{bc} in controlling ventricular CSF sodium concentration (Fig. 5). Total-effect sensitivity indices, which account for total contribution of the inputs to variations in the model response, should be used to compare the significance of the model inputs in controlling the model output. P_{cp} has a larger S_{Ti} than P_{bc}, which shows P_{cp} is a more influential parameter in the model.

Figure 5.

Total-effect sensitivity indices of some of the parameters are smaller than 0.01 (Fig. 5). This means that the variations of these parameters do not influence the variance of the model output significantly; thus these parameters can be fixed at arbitrary values within their ranges [25, 26]. Figure 6 demonstrates the rank order of the model parameters when the model output was defined as the percent change of total extracerebral sodium concentration within 2 hours after perturbations of P_{cp} and P_{bc}:

Model Output= $\frac{\left(\frac{\int_0^{t_{max}} C_s\, dt}{t_{max}}\right) - C_s(t=0)}{C_s(t=0)}$.

Our results indicate that P_{cp} is the most sensitive parameter in controlling extracerebral sodium concentration (Fig. 6). P_{bc} is the second most sensitive parameter in the model. The fact that P_{bc} is more important in influencing extracerebral sodium concentration than ventricular sodium concentration (Figs. 5-6) is because variations in P_{bc} not only can affect sodium exchange at the contact surface of extracerebral CSF and brain tissue, but also can influence sodium exchange between the ventricular system and brain tissue, thus affecting the amount of sodium entering the subarachnoid space from the ventricular system.

Figure 6

We also performed a GSA to identify the influential parameters when the model output was the percent change in total concentration of brain sodium after 2 hours of perturbations of P_{cp} and P_{bc}:

Model Output= $\frac{\left(\int_{r_i}^{r_o} C_{br}\, 4\pi r^2 dr\right) - C_{br}(t=0) \times (total\ volume\ of\ brain\ tissue)}{C_{br}(t=0) \times (total\ volume\ of\ brain\ tissue)}$, t= 2 hr.

Our results indicate that P_{cp} is the most sensitive model parameter in controlling brain sodium levels, followed by P_{bc} (Fig. 7). This result implies that sodium exchange between CSF and brain tissue at the contact surface of the ventricular system and brain tissue, as well as at the contact surface of the subarachnoid space and brain tissue can significantly influence brain sodium levels during migraines.

Figure 7.

Our findings reveal that the variations of P_{bc} affect the brain tissue sodium levels and extracerebral sodium concentrations more than the ventricular sodium concentration (Figs. 5-7).

To further investigate the dynamics of sodium exchange between the CSF and ISF at the interface of brain tissue and the ventricular system, and at the contact surface of brain tissue and subarachnoid space during an episode of migraine, we randomly sampled 10^5 sets of parameters, following a uniform distribution over a 14-dimensional parameter space, and compared the average absolute sodium flux (q_v) between ISF and ventricular CSF, with the average absolute sodium flux (q_s) between the ISF and extracerebral CSF. The average absolute fluxes q_v and q_s are defined by

$$q_v = \frac{\int_0^{t_{max}} \left| P_{vb}\lambda(C_v - \frac{C_{br}(t, r_i)}{V_{br}}) \right| dt}{t_{max}}$$

$$q_s = \frac{\int_0^{t_{max}} \left| P_{sb}\lambda(C_s - \frac{C_{br}(t, r_o)}{V_{br}}) \right| dt}{t_{max}} \quad ,$$

where $t_{max} = 2$ h. Figure 8 shows the ratio of q_v to q_s for the 10^5 randomly sampled parameters. Our results indicate that the ratio of q_v to q_s is greater than 1 for the majority of the samples, which indicates that the absolute sodium flux at the interface of the ventricular system and the brain tissue is greater than the absolute sodium flux at the contact surface of the subarachnoid space and the brain tissue.

Figure 8.

Discussion

Previous studies [2, 3] have indicated that migraine sufferers have higher levels of CSF and ISF sodium than the control group. However, plasma levels of sodium remain unchanged during migraine [2]. Under the hypothesis that these elevated levels are due to variations in the activity levels of NKATs on the epithelial cells of the CP and/or on the endothelial cells of brain capillaries, we investigated the significance of variations of the activity levels of NKATs in controlling CSF and ISF sodium concentrations. In this regard, first we developed a computational model for sodium exchange between different brain compartments, i.e. plasma, brain tissue, ventricular and extracerebral CSF. The model presented in this paper is similar in many respects to that of Smith and Rapoport [8]. However, there are two major differences between our model and theirs. First, our model includes the ventricular system and subarachnoid space as separate compartments. Thus, our model can distinguish between the ventricular and extracerebral CSF, as well as provide insight into the dynamics of sodium exchange between the CSF and ISF at the interface of brain tissue and the ventricular system, and at the contact surface of brain tissue and the subarachnoid space. Second, we have proposed a more realistic model of brain tissue compared to previous studies [8, 11, 27]. Unlike previous studies that modeled brain tissue as a rectangular sheet bathed on two opposite sides by CSF, we modeled brain tissue as the area between two concentric spheres. In our model the contact surface area of the brain tissue and the subarachnoid space is larger than that of the brain tissue and the ventricular system. Thus, sodium exchange between the CSF and brain tissue at the two contact surfaces, as well as sodium diffusion in the brain ISF were modeled more accurately in this paper than in previous studies. We assumed that there is no rate-limiting diffusion between the CSF and brain ISF at the two contact surfaces of the CSF and ISF. This results in instantaneous equilibrium between CSF sodium concentration and ISF sodium concentration at the contact surface of brain tissue and CSF [8]. We also ignored sodium transport between the CSF and ISF via convection due to the small flow rate of CSF from the ventricular system and the subarachnoid space to the brain ISF, as compared to the CSF flow rate from the ventricular system to the subarachnoid space, and the CSF elimination rate in the subarachnoid space [28, 29].

We performed a global sensitivity analysis to compare the significance of CP and CEC NKATs in controlling CSF and brain sodium levels. The effects of variations in the activity levels of CP and

CEC NKATs were modeled as changes in the permeability coefficients of CP and CEC to sodium. Our simulation results indicate that the variation of P_{cp} is more important than that of P_{bc} in controlling CSF and ISF sodium concentrations. Our results were obtained using GSA, which gives us some insight into the importance of P_{cp} and P_{bc} in controlling CSF and ISF sodium by covering the entire parameter space, where all model parameters can vary within the specified ranges. Thus, in a rat model, the intrinsic variations between a population of rats of the same type were considered in this work.

This study has some limitations. First, we compared the importance of variations of the activity levels of CP and CEC NKATs in controlling ISF sodium concentrations. This is because altered ISF sodium levels can induce neuronal excitability and can cause migraine. However, the pathophysiology of migraine is not fully known, and migraine can have different triggers. Various migraine triggers can change the activity levels of NKATs to different extents. The current study cannot predict the extent of variations in CP and CEC NKAT activity levels during an episode of migraine with a particular trigger. For example, one migraine trigger can change the activity of CEC NKATs much more than CP NKATs, whereas another trigger may work conversely. Further studies about how and to what extent different migraine triggers affect NKAT activity levels are needed to better understand the roles of CP and CEC NKATs in migraine onset and propagation. Second, for simplicity, we modeled the rat brain with three spheres. However, the geometry of a rat brain is much more complicated. A more realistic model of the brain and ventricles can provide a better understanding of the phenomenon under study. Third, we modeled the CSF with two well-mixed compartments, i.e. the ventricular system and the subarachnoid space. However, CSF flows through the lateral ventricles, the third ventricle, the cerebral aqueduct, the fourth ventricle, the cisterns and the subarachnoid space. Sodium concentration can vary slightly to significantly from one ventricle to another one and to the subarachnoid space. Thus, the current model can be improved to include all of the ventricles and subarachnoid space as separate compartments. To do this, further information regarding the dynamics of sodium transport between different ventricles and adjacent brain tissues is needed. Next, for simplicity in this model we estimated the ISF sodium concentration by $\frac{C_{br}}{V_{br}}$. This implies that the intracellular sodium concentration reaches equilibrium with the extracellular sodium concentration at a time scale equal to or smaller than the time scale of sodium diffusion in the ISF [8]. In other words, the ratio of extracellular sodium concentration

to intracellular sodium concentration remains unchanged at any time after perturbation of P_{cp} and P_{bc}. The dynamics of sodium exchange between the brain cells and the ISF can be better understood by adding the brain cells as a new compartment to the current model. Our model can be expanded to include brain cells once more information becomes available regarding the permeability coefficients of brain cells to sodium. Finally, we perturbed P_{cp} and P_{bc} at t=0 and kept them unchanged during the experiment time (2 hours). However, in reality, CP and CEC permeability coefficients can change over time. For instance, in a nitroglycerin (NTG) migraine model in the rats, activity levels of CP and CEC NKATs are likely functions of plasma concentration of NTG, and the activity levels return back to their normal levels once the effect of the drug is gone. Thus, the model presented in this study can be used to study the contribution of CP and CEC NKATs to variations in the ISF and CSF sodium concentrations once there is more information about time-dependent activity levels of NKATs during an episode of migraine with a particular trigger.

Conclusions

Our theoretical mechanism for migraine implies that a disturbance in brain sodium homeostasis causes migraine. This sodium dysregulation is most likely due to overactivity of NKATs on the CP and CEC. Unfortunately, understanding migraine pathophysiology is difficult, not only because migraines have different triggers in different people, but also because the effects of various triggers on activity levels of CP and CEC NKATs are not known. To approach this problem, we used mechanistic modeling together with global sensitivity analysis (GSA) to assess the relative importance of CP and CEC NKATs in controlling CSF and ISF sodium concentrations. GSA provides insight into the significance of CP and CEC NKATs in regulating brain sodium concentration when the exact extent of overactivity of CP and CEC NKATs is unknown. Our simulation results show that CP NKATs are more important than CEC NKATs in controlling ISF and CSF sodium concentrations. It is important to note that our results were obtained using GSA which covers the entire region of parameter space. However, it might be possible that for a specific migraine trigger, CEC NKATs contribute more than CP NKATs to the regulation of CSF and/or ISF sodium concentrations. In summary, this study suggests that correcting the altered homeostasis of CP NKATs can potentially normalize brain sodium dysregulation and subsequently treat most

migraines with various triggers. This prediction needs to be verified experimentally for various types of migraines. The model presented in this study can guide the design of further experimental studies, as well as provide insight for further computational studies.

Abbreviations

CSF: Cerebrospinal fluid

ISF: Brain interstitial fluid

CEC: Capillary endothelial cells

CP: Choroid plexus

NKAT: Na^+, K^+-ATPase

GSA: Global sensitivity analysis

NTG: Nitroglycerin

Supplementary Information

Global Sensitivity Analysis

In this work, we used a MATLAB toolbox called SAFE [18] to perform a global sensitivity analysis (GSA). SAFE implements several GSA methods such as the Elementary Effects Test, Regional Sensitivity Analysis, and Sobol's technique. Sobol's method is a variance-based global sensitivity analysis technique which evaluates the sensitivity of the solutions with respect to the model parameters as well as the interactions between different parameters. Using the principles of variance decomposition, Sobol's method ranks the parameters in terms of their importance. Given an integrable function f over a p-dimensional parameter space Ω^p,

$$y = f(x_1, x_2, \dots, x_p) \tag{S1}$$

Each parameter can vary within a finite range. Sobol's method considers expansion of the response into a set of functions of increasing dimensionality,

$$f(x) = f_0 + \sum_{i=1}^{p} f_i + \sum_{i=1}^{p} \sum_{j>i}^{p} f_{ij} + \cdots + f_{123\dots p}\,, \tag{S2}$$

where each individual term is a function of the parameters in its index. The total variance of the function output is defined by

$$D(y) = \int_{\Omega^p} f^2(x)\, dx - \left(\int_{\Omega^p} f(x)\, dx \right)^2 . \tag{S3}$$

Sobol's technique is based on decomposition of the total variance D into partial variances indicating the contributions from effects of individual parameters and combined effects of pairs of parameters. This decomposition is accomplished using the expansion of f into terms of increasing dimensions (Eq. S2),

$$D(y) = \sum_{i=1}^{p} D_i(y) + \sum_{i=1}^{p} \sum_{j>i}^{p} D_{ij}(y) + \cdots + D_{123\dots p}(y)\,. \tag{S4}$$

According to Sobol's method, the first-order sensitivity index for each parameter is given by

$$S_i = \frac{D_i(y)}{D(y)}, \tag{S5}$$

The first-order sensitivity index accounts for the main individual contribution of each model parameter to the variance of the model output. The Sobol's total-effect index, on the other hand, represents total contribution of the input to the response variation. The total-effect index for parameter x_i is calculated by the sum of all sensitivity indices which have i in their index

$$S_{Ti} = S_i + \sum_{i \neq j} S_{ij} + \sum_{i \neq j, i \neq l, j < l} S_{ijl} + \cdots \tag{S6}$$

Based on Sobol's approach, the necessary and sufficient condition for parameter x_i to be a noninfluential factor is $S_{Ti} = 0$. However, previous studies have indicated that a parameter can be considered noninfluential if its total-effect sensitivity index is smaller than 0.01, and significantly smaller than total-effect sensitivity indices of the rest of the parameters [25, 26, 30, 31].

Fig. 1

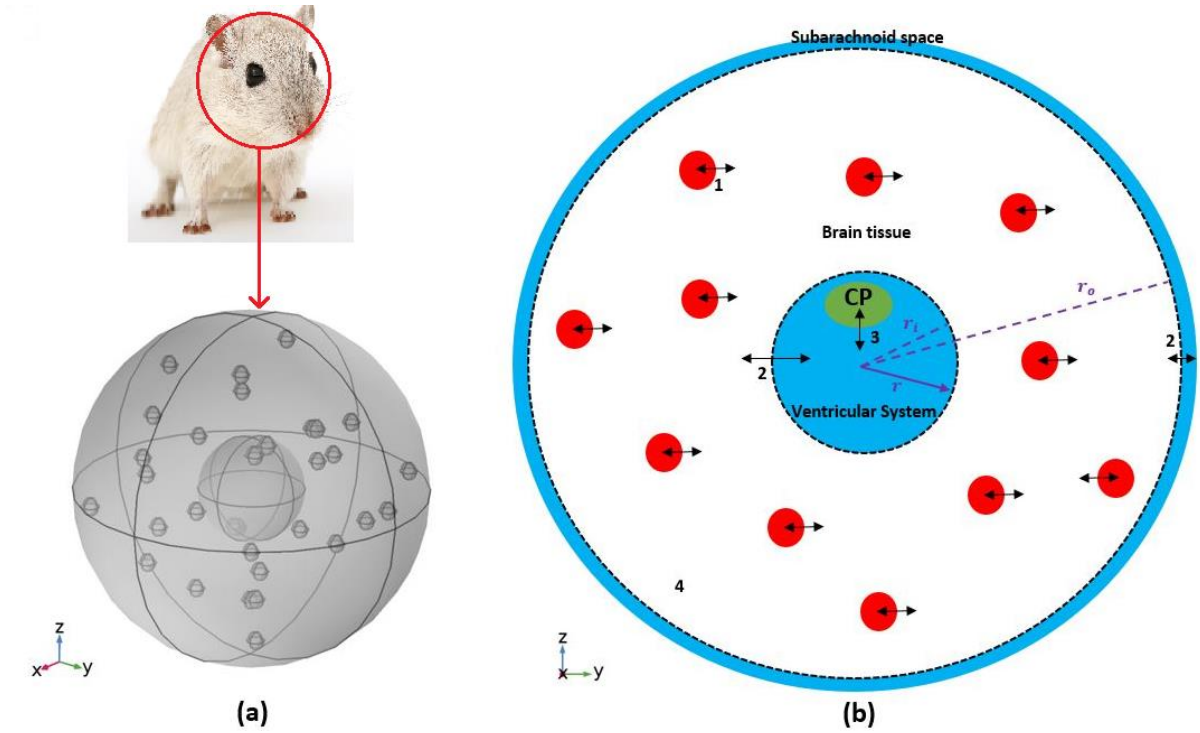

Figure 1. Schematic of the model. (a) A 3D model of a rat's brain. (b) A 2D view of the cross section of the 3D model. The inner circle, shown in blue, represents the ventricular system, while the outer ring, shown in blue, is subarachnoid space. The white region between two dashed circles is brain tissue. Blood vessels, shown in red circles, are distributed uniformly in the brain tissue. The CP is depicted by a green ellipsoid. Numbers in the figure specify the types and locations of sodium transport: 1. capillary-brain transport; 2. free exchange between CSF and ISF; 3. blood-CSF exchange at the CP; 4. diffusive transport across brain ISF.

Fig. 2a

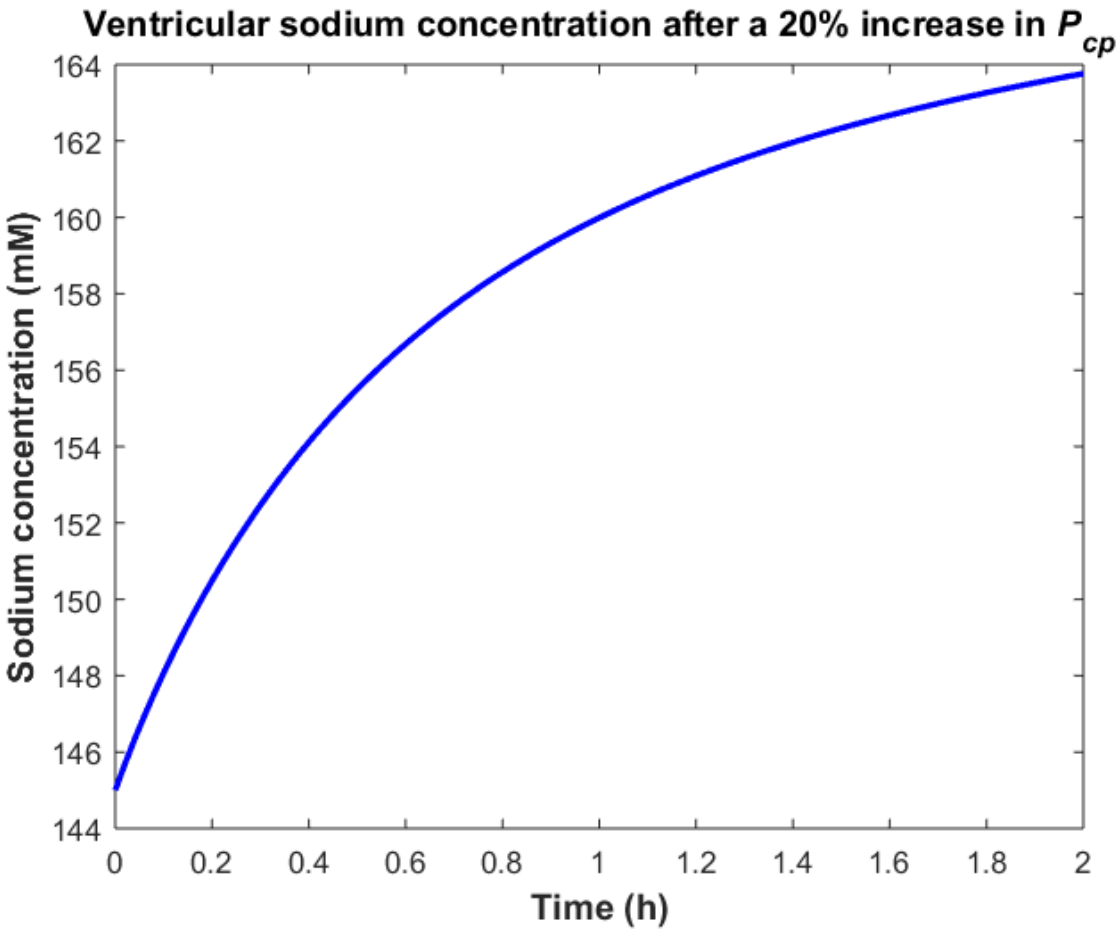
Ventricular sodium concentration after a 20% increase in P_{cp}
Sodium concentration (mM)
164
162
160
158
156
154
152
150
148
146
144
0
0.2
0.4
0.6
0.8
1
1.2
1.4
1.6
1.8
2
Time (h)

Fig. 2b

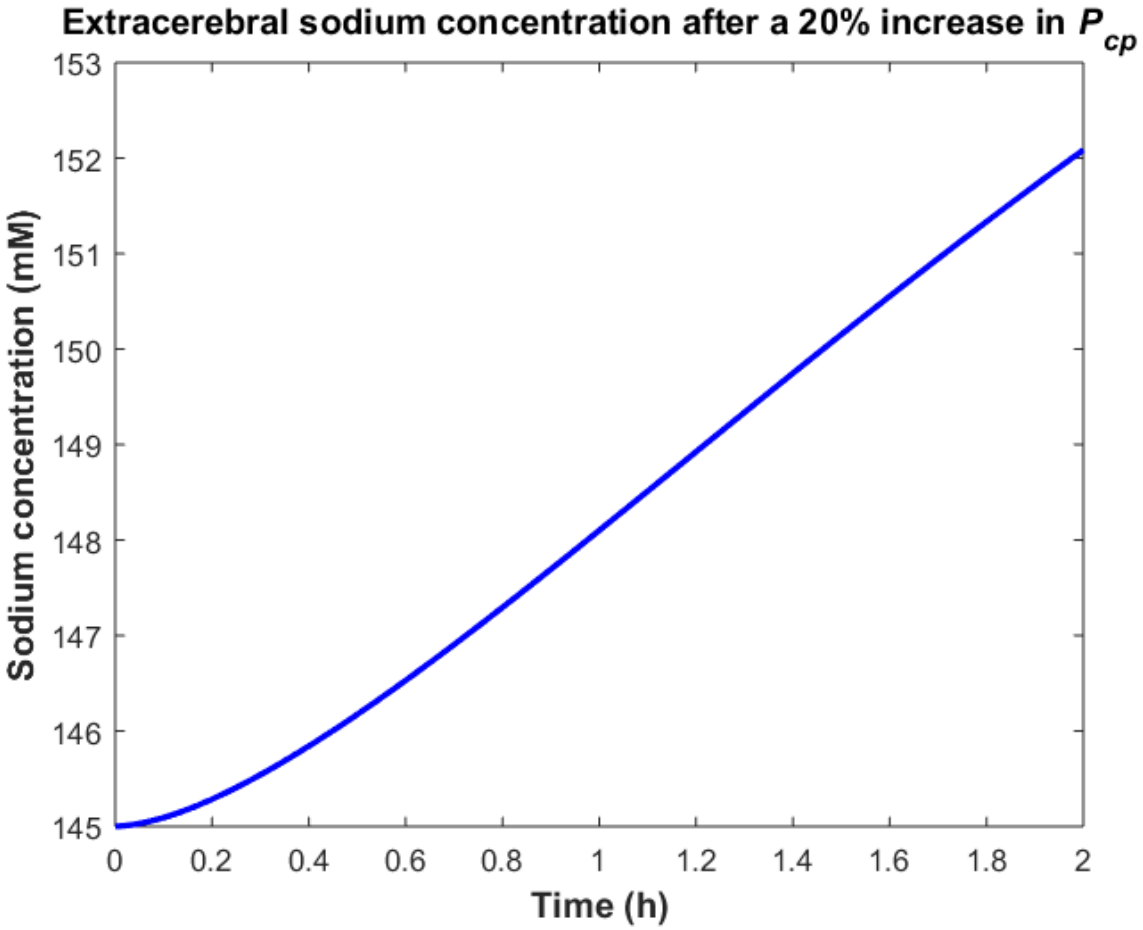
Extracerebral sodium concentration after a 20% increase in P_{cp}
Sodium concentration (mM)
153
152
151
150
149
148
147
146
145
0
0.2
0.4
0.6
0.8
1
1.2
1.4
1.6
1.8
2
Time (h)

Fig. 2c

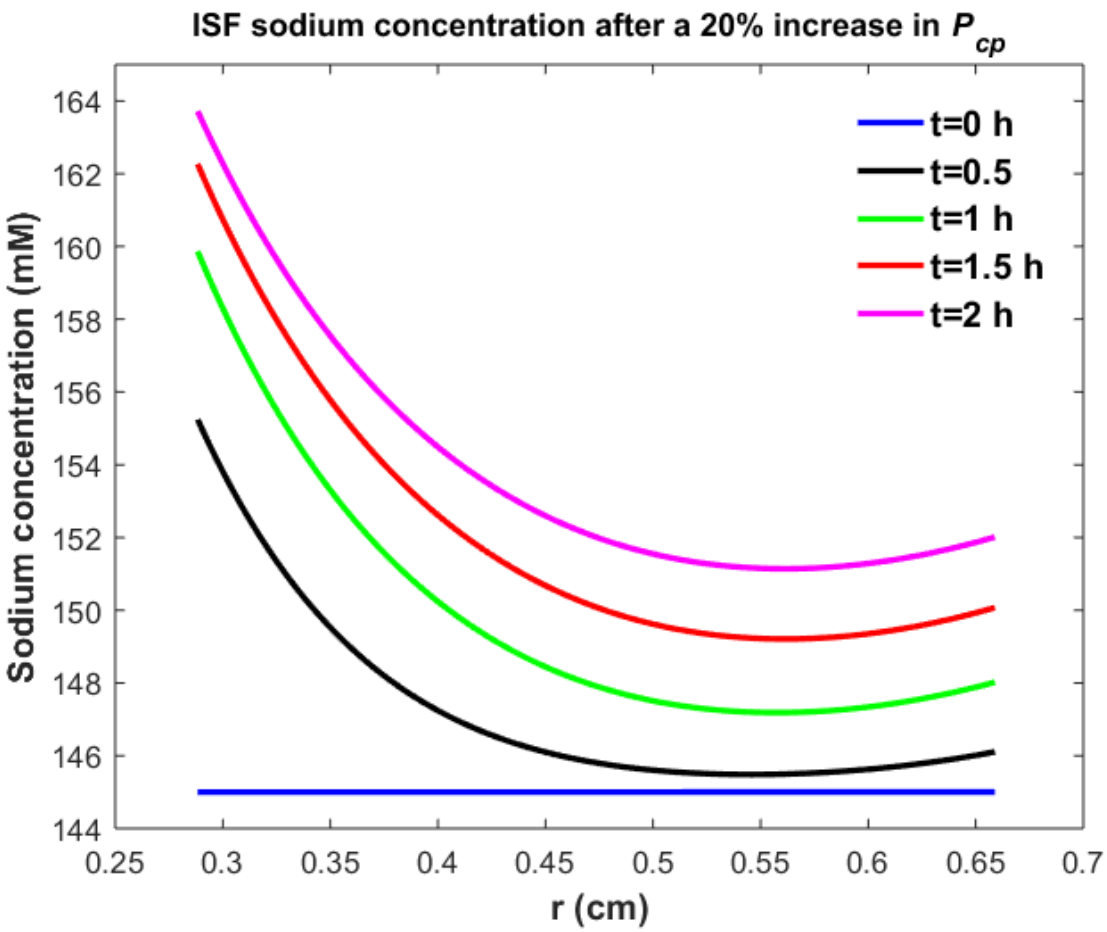

Figure 2. Variations of (a) C_v, (b) C_s and (c) C_{br} within two hours after increasing P_{cp} by 20%.

Fig. 3a

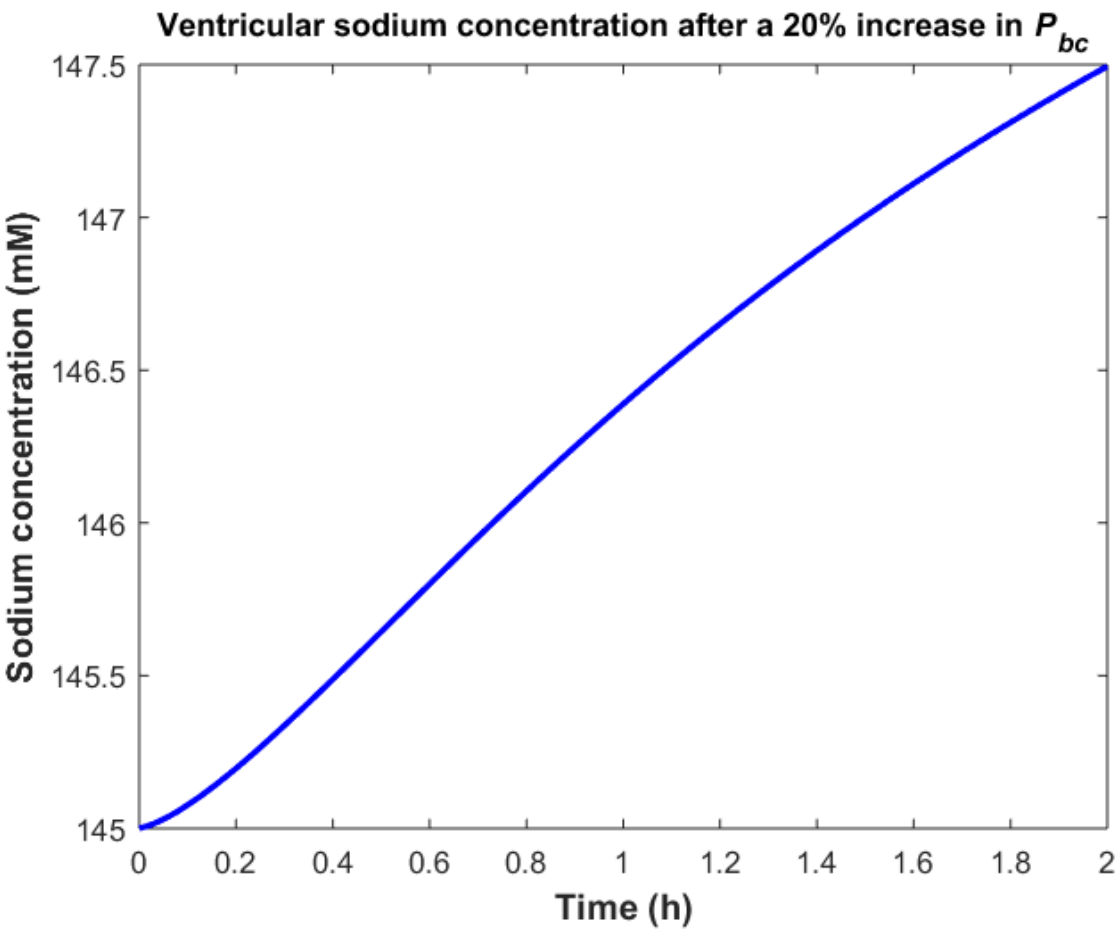
Ventricular sodium concentration after a 20% increase in P_{bc}
Sodium concentration (mM)
147.5
147
146.5
146
145.5
145
0
0.2
0.4
0.6
0.8
1
1.2
1.4
1.6
1.8
2
Time (h)

Fig. 3b

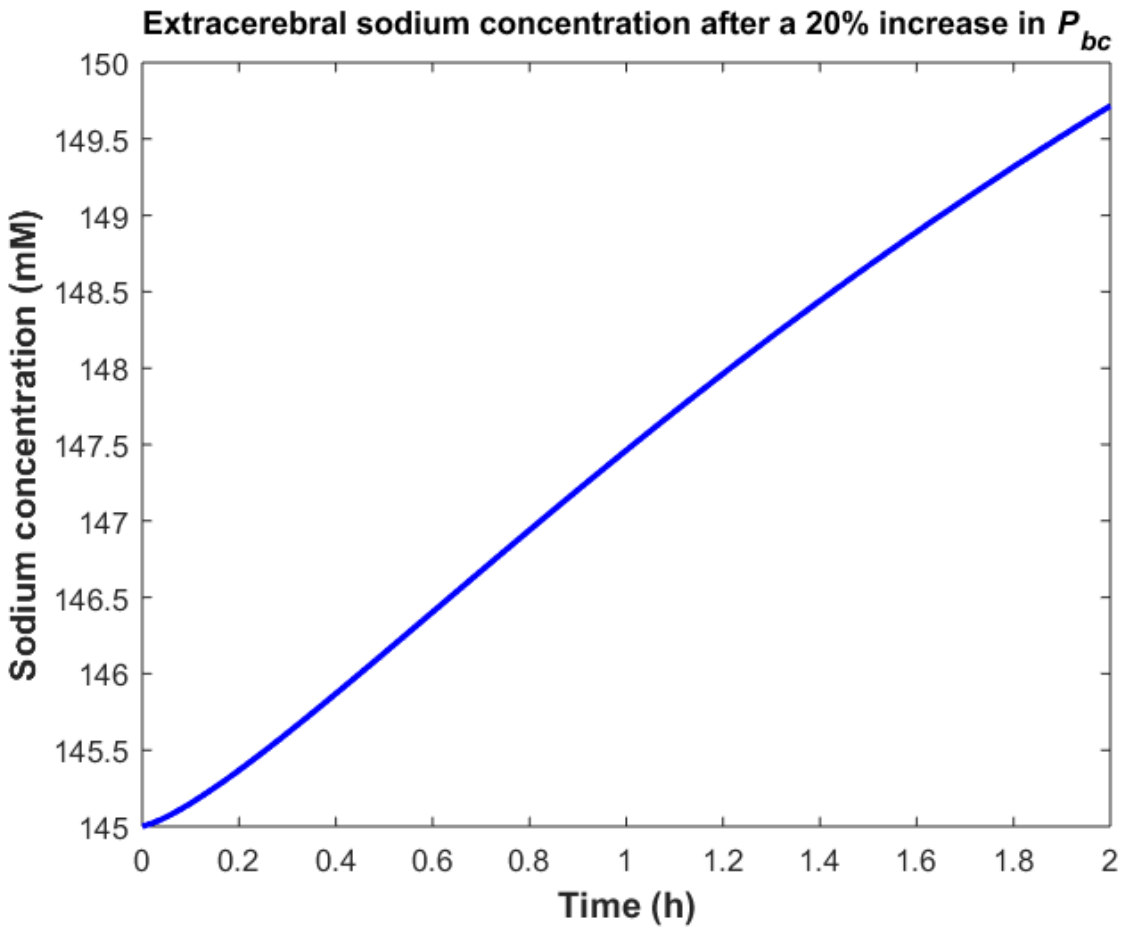
Extracerebral sodium concentration after a 20% increase in P_{bc}
Sodium concentration (mM)
150
149.5
149
148.5
148
147.5
147
146.5
146
145.5
145
0
0.2
0.4
0.6
0.8
1
1.2
1.4
1.6
1.8
2
Time (h)

Fig. 3c

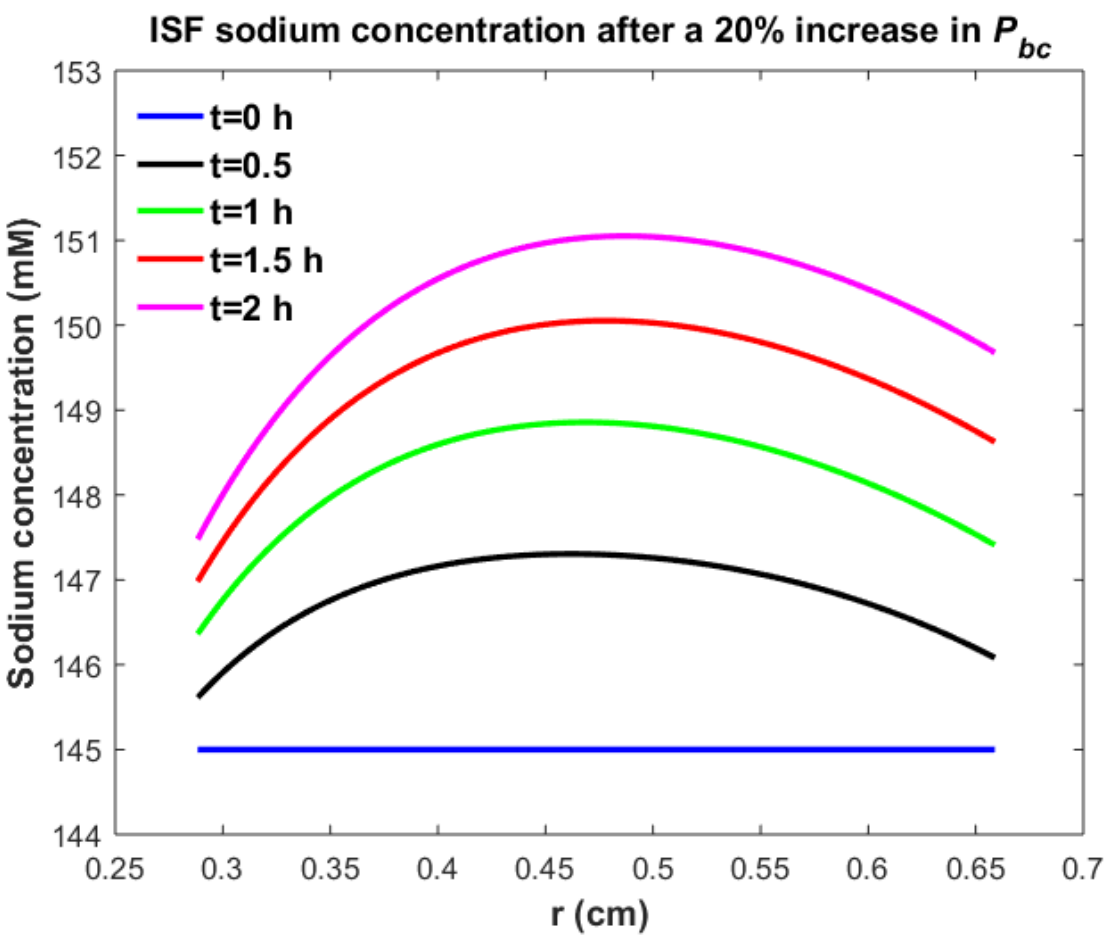

Figure 3. Variations in (a) C_v, (b) C_s and (c) C_{br} after increasing P_{bc} by 20%.

Fig. 4a

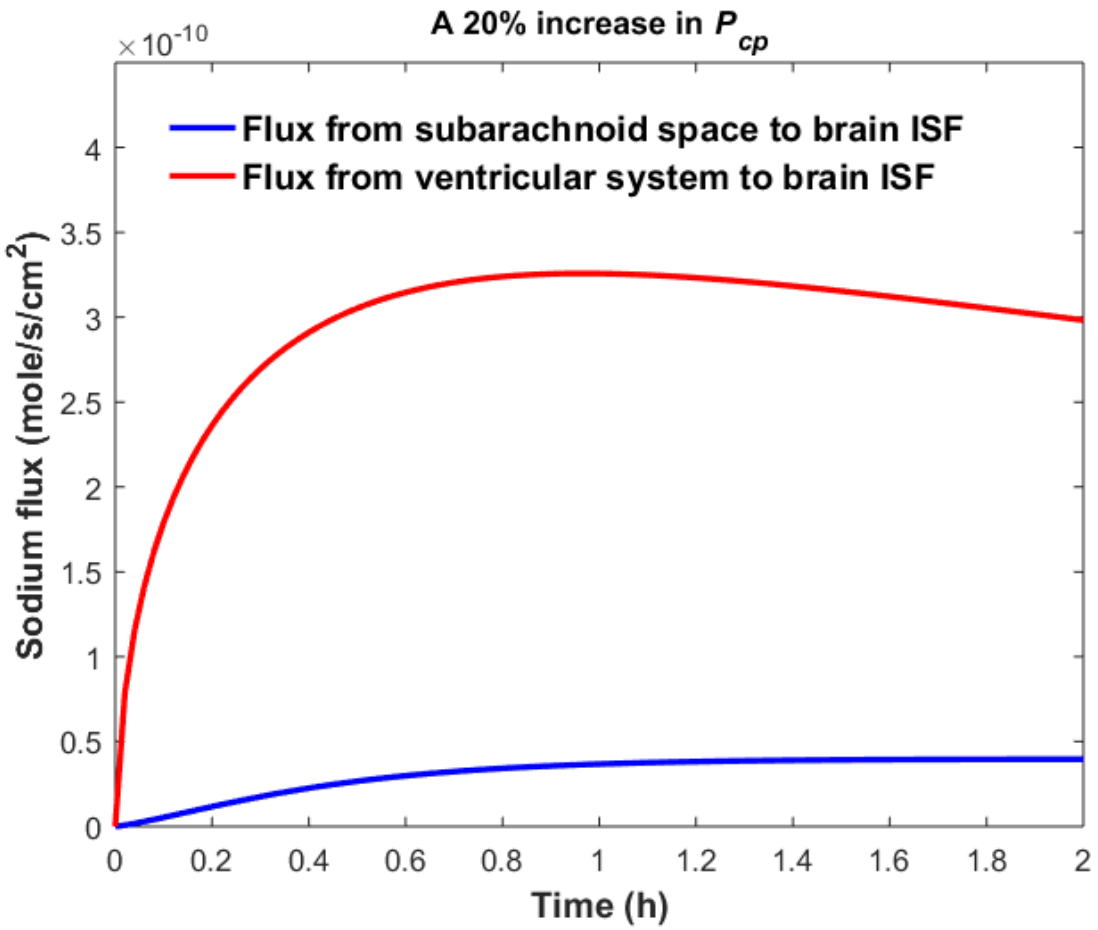
A 20% increase in P_{cp}
$\times 10^{-10}$
Flux from subarachnoid space to brain ISF
Flux from ventricular system to brain ISF
Sodium flux (mole/s/cm^2)
Time (h)
0
0.5
1
1.5
2
2.5
3
3.5
4
0
0.2
0.4
0.6
0.8
1
1.2
1.4
1.6
1.8
2

Fig. 4b

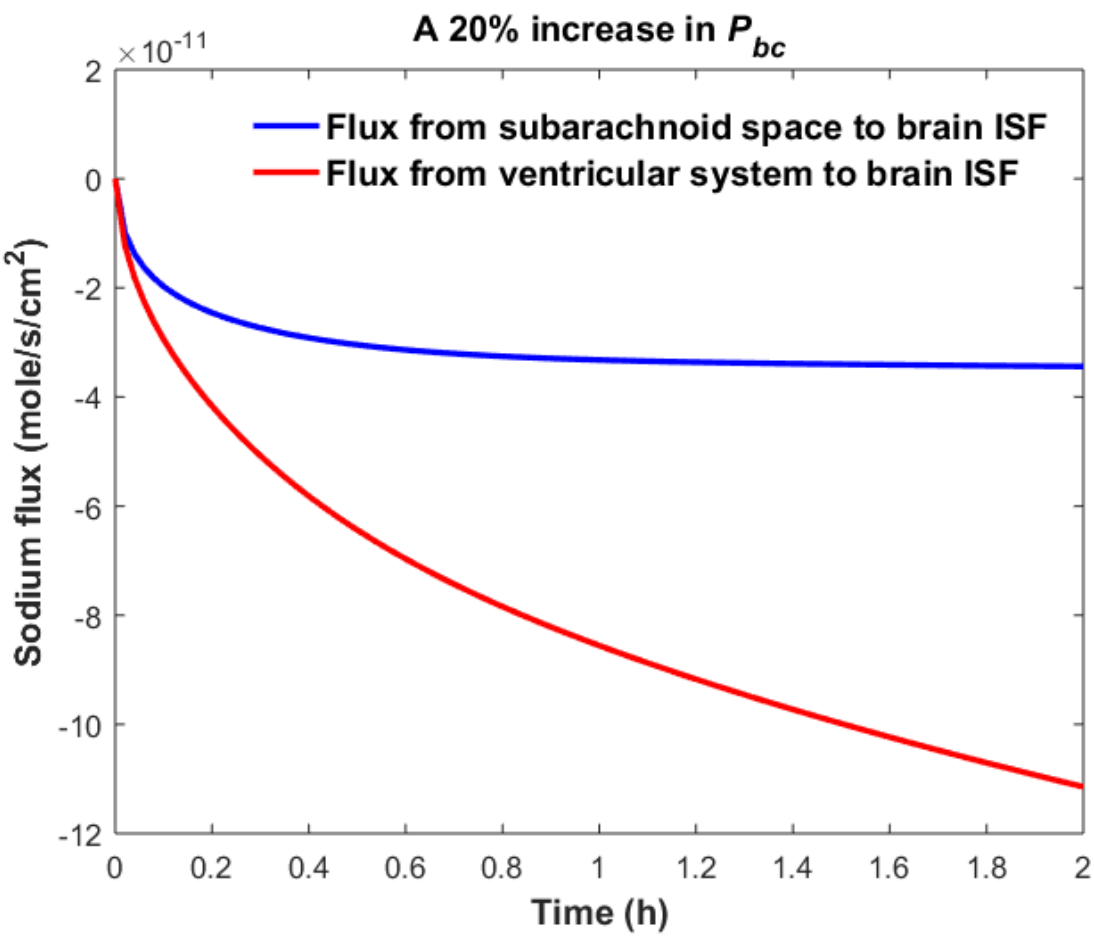

Figure 4. Comparison of sodium flux at the interface of the brain tissue and the ventricular system with sodium flux at the interface of the brain tissue and the subarachnoid space after increasing (a) P_{cp} and (b) P_{bc} by 20%. The positive sign of the flux indicates that sodium is diffusing from the CSF to the brain ISF, while the negative sign indicates that sodium is diffusing from the brain ISF to the CSF.

Fig. 5

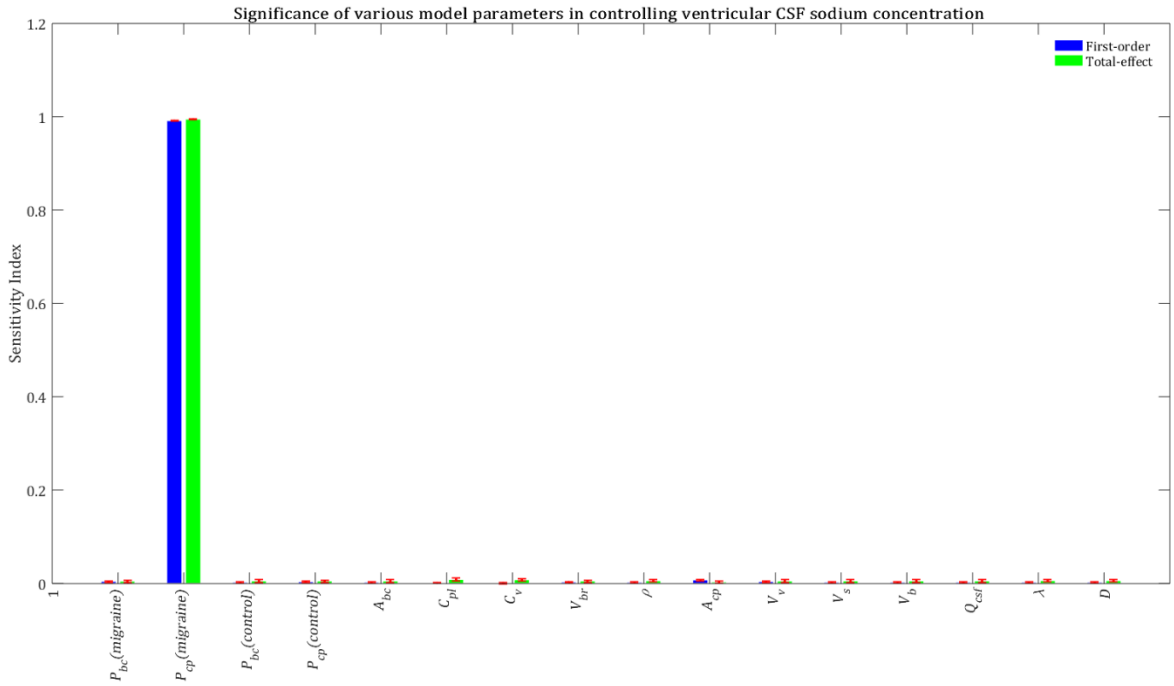

Figure 5. Sensitivity ranking of the model parameters. The model output was set to the time integral of C_v within 2 hours after perturbation of the model's parameters. The blue bars represent first-order sensitivity indices, while the green bars show the total-effect sensitivity indices. The error bars, shown in red, indicate the bootstrap confidence intervals (95% confidence intervals) of the mean values.

Fig. 6

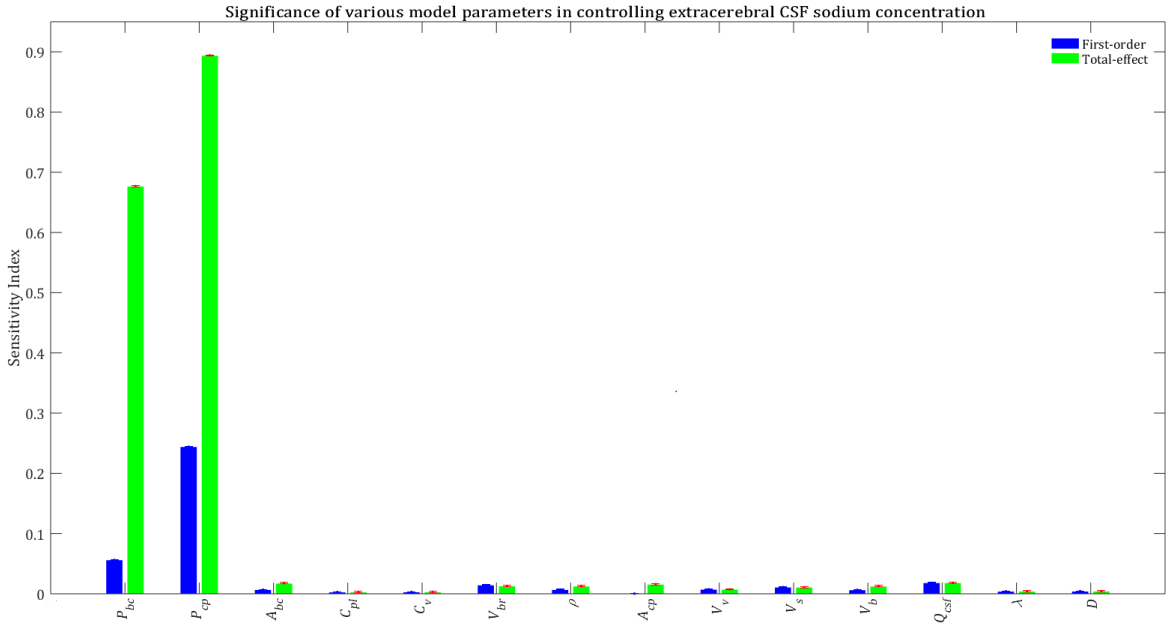

Figure 6. Relative significance of the model parameters in controlling extracerebral sodium concentration (C_s). The blue bars represent first-order sensitivity indices, while the green bars show the total-effect sensitivity indices. The error bars, shown in red, indicate the bootstrap confidence intervals (95% confidence intervals) of the mean values.

Fig. 7

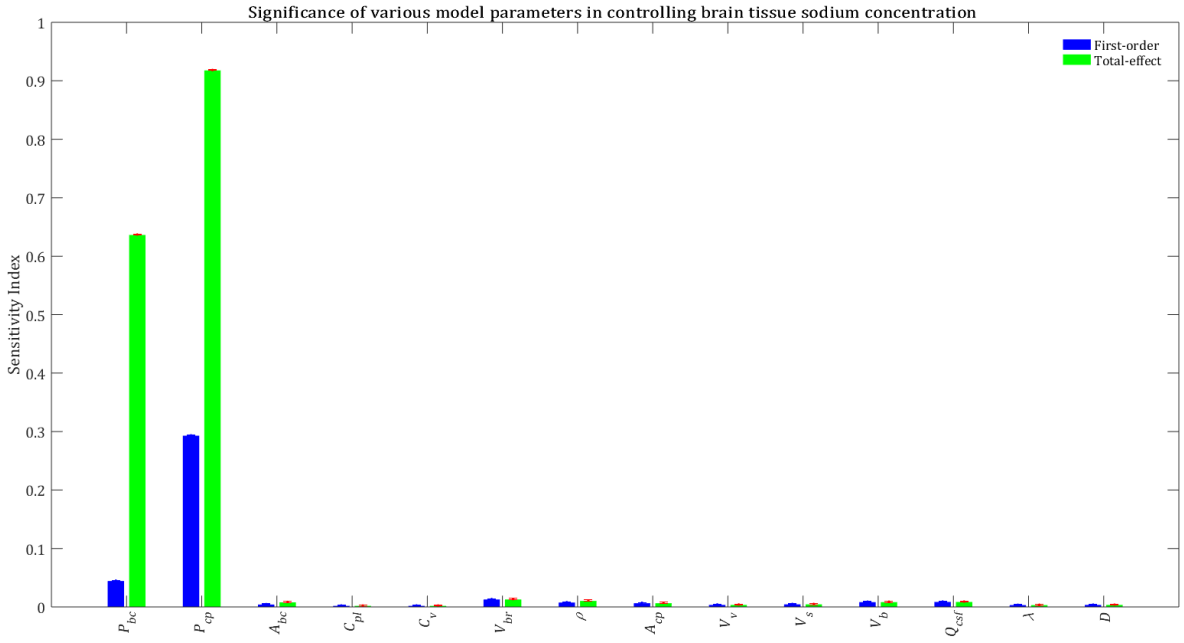

Figure 7. Relative importance of the model parameters in controlling ISF sodium concentration. The blue bars represent first-order sensitivity indices, while the green bars show the total-effect sensitivity indices. The error bars, shown in red, indicate the bootstrap confidence intervals (95% confidence intervals) of the mean values.

Fig. 8

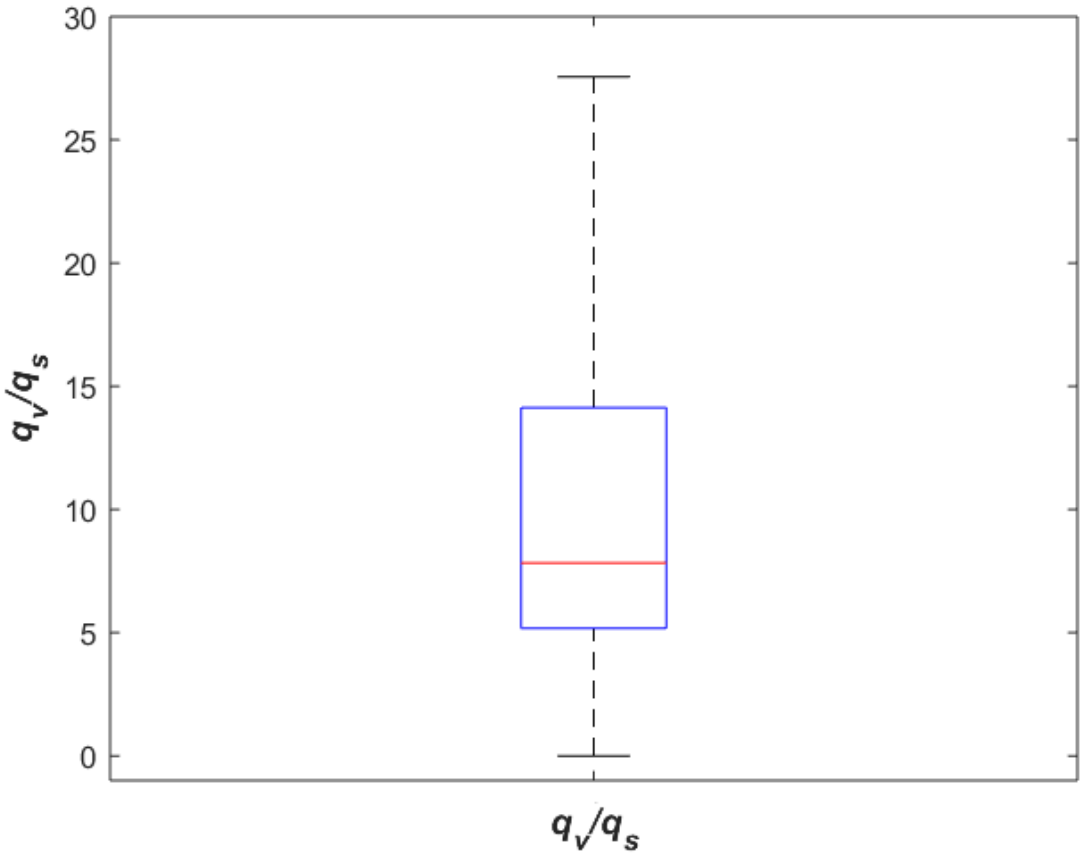

Figure 8. The ratio of absolute sodium flux at the interface of the ventricular system and the brain tissue (q_v) to absolute sodium flux at the interface of the subarachnoid space and the brain tissue (q_s). 10^5 points were sampled randomly following a uniform distribution to generate this Figure.

References

1. Steiner TJ, Stovner LJ, Vos T, Jensen R, Katsarava Z: Migraine is first cause of disability in under 50s: will health politicians now take notice? In.; 2018.
2. Harrington MG, Fonteh AN, Cowan RP, Perrine K, Pogoda JM, Biringer RG, Hühmer AF: Cerebrospinal fluid sodium increases in migraine. Headache: The Journal of Head and Face Pain 2006, 46(7):1128-35.
3. Abad N, Rosenberg JT, Hike DC, Harrington MG, Grant SC: Dynamic sodium imaging at ultra-high field reveals progression in a preclinical migraine model. Pain 2018, 159(10):2058-65.
4. Harrington MG, Chekmenev EY, Schepkin V, Fonteh AN, Arakaki X: Sodium MRI in a rat migraine model and a NEURON simulation study support a role for sodium in migraine. Cephalalgia 2011, 31(12):1254-65.
5. Arakaki X, Foster H, Su L, Do H, Wain AJ, Fonteh AN, Zhou F, Harrington MG: Extracellular sodium modulates the excitability of cultured hippocampal pyramidal cells. Brain research 2011, 1401:85-94.
6. Hodgkin AL, Katz B: The effect of sodium ions on the electrical activity of the giant axon of the squid. The Journal of physiology 1949, 108(1):37-77.
7. Harrington MG, Fonteh AN, Arakaki X, Cowan RP, Ecke LE, Foster H, Hühmer AF, Biringer RG: Capillary endothelial Na+, K+, ATPase transporter homeostasis and a new theory for migraine pathophysiology. Headache: The Journal of Head and Face Pain 2010, 50(3):459-78.
8. Smith QR, Rapoport SI: Cerebrovascular permeability coefficients to sodium, potassium, and chloride. Journal of neurochemistry 1986, 46(6):1732-42.
9. Aminfar A, Davoodzadeh N, Aguilar G, Princevac M: Application of optical flow algorithms to laser speckle imaging. Microvascular research 2019, 122:52-9.
10. Davoodzadeh N, Halaney D, Jonak CR, Cuando N, Aminfar A, Binder DK, Aguilar G: Laser speckle imaging of brain blood flow through a transparent nanocrystalline yttria-stabilized-zirconia cranial implant. In: Dynamics and Fluctuations in Biomedical Photonics XV: 2018. International Society for Optics and Photonics: 1049303.
11. Collins JM, Dedrick RL: Distributed model for drug delivery to CSF and brain tissue. American Journal of Physiology-Regulatory, Integrative and Comparative Physiology 1983, 245(3):R303-R10.
12. Brøchner CB, Holst CB, Møllgård K: Outer brain barriers in rat and human development. Frontiers in neuroscience 2015, 9:75.
13. Sahin B, Aslan H, Unal B, Canan S, Bilgic S, Kaplan S, Tumkaya L: Brain volumes of the lamb, rat and bird do not show hemispheric asymmetry: a stereological study. Image Analysis & Stereology 2011, 20(1):9-13.
14. Goodman JA, Kroenke CD, Bretthorst GL, Ackerman JJ, Neil JJ: Sodium ion apparent diffusion coefficient in living rat brain. Magnetic Resonance in Medicine: An Official Journal of the International Society for Magnetic Resonance in Medicine 2005, 53(5):1040-5.
15. Lei Y, Han H, Yuan F, Javeed A, Zhao Y: The brain interstitial system: Anatomy, modeling, in vivo measurement, and applications. Progress in neurobiology 2017, 157:230-46.
16. Bito L, Davson H: Local variations in cerebrospinal fluid composition and its relationship to the composition of the extracellular fluid of the cortex. Experimental neurology 1966, 14(3):264-80.
17. Olsen NS, Rudolph GG: Transfer of sodium and bromide ions between blood, cerebrospinal fluid and brain tissue. American Journal of Physiology-Legacy Content 1955, 183(3):427-32.

18. Pianosi F, Sarrazin F, Wagener T: A Matlab toolbox for global sensitivity analysis. Environmental Modelling & Software 2015, 70:80-5.
19. Kim KA, Spencer SL, Albeck JG, Burke JM, Sorger PK, Gaudet S: Systematic calibration of a cell signaling network model. BMC bioinformatics 2010, 11(1):202.
20. Zhang XY, Birtwistle M, Gallo J: A General Network Pharmacodynamic Model–Based Design Pipeline for Customized Cancer Therapy Applied to the VEGFR Pathway. CPT: pharmacometrics & systems pharmacology 2014, 3(1):1-9.
21. Ghaffari H, Petzold LR: Identification of influential proteins in the classical retinoic acid signaling pathway. Theoretical Biology and Medical Modelling 2018, 15(1):16.
22. Sumner T, Shephard E, Bogle I: A methodology for global-sensitivity analysis of time-dependent outputs in systems biology modelling. Journal of The Royal Society Interface 2012, 9(74):2156-66.
23. Zhang XY, Trame M, Lesko L, Schmidt S: Sobol sensitivity analysis: a tool to guide the development and evaluation of systems pharmacology models. CPT: pharmacometrics & systems pharmacology 2015, 4(2):69-79.
24. Ghaffari H, Varner JD, Petzold LR: Analysis of the role of thrombomodulin in all-trans retinoic acid treatment of coagulation disorders in cancer patients. Theoretical Biology and Medical Modelling 2019, 16(1):3.
25. Tang T, Reed P, Wagener T, Van Werkhoven K: Comparing sensitivity analysis methods to advance lumped watershed model identification and evaluation. Hydrology and Earth System Sciences Discussions 2006, 3(6):3333-95.
26. Sin G, Gernaey KV, Neumann MB, van Loosdrecht MC, Gujer W: Global sensitivity analysis in wastewater treatment plant model applications: prioritizing sources of uncertainty. Water research 2011, 45(2):639-51.
27. Davson H, Welch K: The permeation of several materials into the fluids of the rabbit's brain. The Journal of physiology 1971, 218(2):337-51.
28. Abbott NJ: Evidence for bulk flow of brain interstitial fluid: significance for physiology and pathology. Neurochemistry international 2004, 45(4):545-52.
29. Pardridge WM: Drug transport in brain via the cerebrospinal fluid. Fluids and Barriers of the CNS 2011, 8(1):7.
30. Ghaffari H, Saidi MS, Firoozabadi B: Biomechanical analysis of actin cytoskeleton function based on a spring network cell model. Proceedings of the Institution of Mechanical Engineers, Part C: Journal of Mechanical Engineering Science 2017, 231(7):1308-23.
31. Cosenza A, Mannina G, Vanrolleghem PA, Neumann MB: Global sensitivity analysis in wastewater applications: A comprehensive comparison of different methods. Environmental modelling & software 2013, 49:40-52.